Journal Pre-proofs

UV/VIS imaging-based PAT tool for drug particle size inspection in intact tablets supported by pattern recognition neural networks

Lilla Alexandra Mészáros, Attila Farkas, Lajos Madarász, Rozália Bicsár, Dorián László Galata, Brigitta Nagy, Zsombor Kristóf Nagy

PII: S0378-5173(22)00328-3
DOI: https://doi.org/10.1016/j.ijpharm.2022.121773
Reference: IJP 121773

To appear in: *International Journal of Pharmaceutics*

Received Date: 22 January 2022
Revised Date: 9 April 2022
Accepted Date: 22 April 2022

Please cite this article as: L. Alexandra Mészáros, A. Farkas, L. Madarász, R. Bicsár, D. László Galata, B. Nagy, Z. Kristóf Nagy, UV/VIS imaging-based PAT tool for drug particle size inspection in intact tablets supported by pattern recognition neural networks, *International Journal of Pharmaceutics* (2022), doi: https://doi.org/10.1016/j.ijpharm.2022.121773

UV/VIS imaging-based PAT tool for drug particle size inspection in intact tablets supported by pattern recognition neural networks

Lilla Alexandra Mészáros[1], Attila Farkas[1], Lajos Madarász[1], Rozália Bicsár[1], Dorián László Galata[1], Brigitta Nagy[1], Zsombor Kristóf Nagy[1*]

[1] Department of Organic Chemistry and Technology, Budapest University of Technology and Economics, H-1111 Budapest, Műegyetem rakpart 3, Hungary

*: corresponding author

zsknagy@oct.bme.hu; Phone: +36-1-463-4129

Abstract

The potential of machine vision systems has not currently been exploited for pharmaceutical applications, although expected to provide revolutionary solutions for in-process and final product testing. The presented paper aimed to analyze the particle size of meloxicam, a yellow model active pharmaceutical ingredient, in intact tablets by a digital UV/VIS imaging-based machine vision system. Two image processing algorithms were developed and coupled with pattern recognition neural networks for UV and VIS images for particle size-based classification of the prepared tablets. The developed method can identify tablets containing finer or larger particles than the target with more than 97% accuracy. Two algorithms were developed for UV and VIS images for particle size analysis of the prepared tablets. According to the applied statistical tests, the obtained particle size distributions were similar to the results of the laser diffraction-based reference method. Digital UV/VIS imaging combined with multivariate data analysis can provide a new non-destructive, rapid, in-line tool for particle size analysis in tablets.

KEYWORDS

image analysis, machine vision, tablet inspection, particle size distribution, particle size analysis, pattern recognition neural network

1. Introduction

Tablets represent a significant portion of the pharmaceutical dosage forms, due to their several advantageous properties, for example, convenient administration, stability, portability, and dosing accuracy [1][2][3]. In 2015, the U.S Food and Drug Administration (FDA) approved the first commercial product, Orkambi by Vertex, manufactured using continuous technology. Thus, the modern manufacturing of pharmaceutical solid dosage forms has begun [4]. Since then, continuous manufacturing, emerging technologies, modernization, and innovation have been the focus of attention and supported by the regulatory agencies [5]. The published recommendations, guidelines, and frameworks, including process analytical technology (PAT) and the concept of quality-by-design (QbD), enable production monitoring and controlling, data collection, and process understanding [6][7].

The initiative of PAT published by the U.S. FDA reinforces the in-line or on-line data-based process control [8][9]. The development of PAT tools can provide consistent quality throughout

the manufacturing by monitoring and controlling process parameters and quality attributes [9]. In the modernization concept, data-driven solutions can contribute to understanding the processes and controlling the intermittent variability to enable consistent quality in each step of the production. These reserve an essential role in implementing QbD and real-time release testing (RTRT) approaches [10].

Particle sizes and the particle size distributions (PSDs) of the components are vital parameters in the pharmaceutical development and manufacturing phases. These critical material attributes (CMAs) affect critical quality attributes (CQAs) and the critical process parameters (CPPs) considering the systematic concept of QbD [11][12][13]. Based on the general quality target product profile (QTPP) of tablets, the content uniformity, *in vitro* dissolution behavior, and bioavailability of the final dosage form, which are more significant related to poorly water soluble APIs, are among the affected CQAs. The time and the blend uniformity are affected CPPs belonging to the homogenization step of the API with excipients, where the particle size of the API potentially represents a high risk. In the compaction step, the compactibility of the powder blends, the compression force, the tensile strength, and the porosity can be affected by the mentioned CMAs [11][12][13].

Consequently, particle sizes and PSDs of the components in tablets significantly affect the efficacy, stability, and safety of the final product. During the production of solid dosage forms, operations are performed, affecting the particle size of the applied materials. Therefore, the monitoring and control of these CMAs are crucial in both powders and the final dosage form throughout the manufacturing [12][11]. The development of real-time, in-line particle size analysis methods in intact tablets can contribute to getting more information about the processes throughout the manufacturing, including tableting[11].

The characterization of a particulate system by PAT tools has been in the attention of industrial companies in the recent decade [9]. There are several methods for the determination of PSDs of powders or granules, such as sieve analysis [14], microscopic measurements [15], sedimentation [16], spectroscopic methods [17], and image analysis [11]. However, only a few publications assess particle sizes and distributions in intact tablets.

Simek et al. applied hot stage microscopy for particle size determination of tablets containing meloxicam and tadalafil as APIs. In the context of the sample preparation methods, destructive mechanical and liquid disintegration was applied [12].

Thakral et al. published a 2-dimensional X-ray diffraction method where the particle size of the API was estimated in intact flat-faced tablets containing lactose-monohydrate and sucrose with different particle sizes. There are a few limitations of this technique, such as the curvature of the surface [11].

Skelbæk-Pedersen et al. investigated the effect of different particle sizes on material fragmentation during the tableting process. They applied diffuse reflectance near-infrared spectroscopic technique and executed a qualitative examination of the particle size of microcrystalline cellulose and calcium hydrogen phosphate dihydrate in tablets using principal component analysis [3].

The most important advantage of the mentioned methods is the capability to examine the particle size of the components in tablets. However, the hot stage microscopic technique appears available for offline analysis of PSD because of the instrumentation, the requirements, and the destructive manner of the sample preparation. The 2-dimensional X-ray diffractometry does not require such sample preparation, although it cannot be applied as a PAT tool due to the instrumentation. Both methods have limitations in the context of the examinable sample number. The U.S. FDA approved the application of near-infrared spectroscopy for in-line measurements despite the mentioned publication only qualitatively examining the particle size in intact tablets.

Machine vision is a specific solution in many fields [18][19][20], which is recently gaining interest in the pharmaceutical industry. It may provide a new, cost-efficient, and rapid way in quality assessment of pharmaceutical products and process control [21]. A few paper reports on the analysis of the final pharmaceutical products, such as tablets. For instance, these mainly focus on monitoring coating processes [8], defects [22], and pellet distribution on the surface of the tablets [23]. According to the authors' knowledge, a machine vision system is not applied for particle size analysis in intact tablets. However, these can assist or supplement other instrumentations and methods in manufacturing and contribute to the process controlling. One of the significant advantages of applying these systems is that all the produced tablets can be examined. The rejected products can be isolated immediately, which reduces the financial loss.

The application of artificial intelligence gained ground in the business processes, the drug development in the pharmaceutical industry and also emerged in the manufacturing of pharmaceutical dosage forms [24][25][26]. Neural networks are nonlinear computational methods that model the communication of neurons in the human brain [27]. These

computational methods are popularly used for approximations and pattern recognition [28]. Pattern recognition neural networks are classifiers and similar in structure to a feed-forward neural network. The difference between them is in the softmax transfer function of the output layer [29]. The application of pattern recognition neural networks can be found in other industrial sectors [30].

This proof-of-concept paper aimed to develop and apply a machine vision system based on digital UV/VIS imaging for qualitative and quantitative particle size assessment of the API in intact tablets. Image processing algorithms were developed, and pattern recognition neural networks were applied for classification based on the different particle sizes of the API. Subsequently, the paper intended to predict the PSD of the API in tablets by combining the classification results and the image processing algorithms. At last, an application example was presented, in which the developed system is introduced for automatic tableting where the tablets included different particle sizes of meloxicam, a yellow model API. The purpose of the final experiment was to determine whether the produced tablets met the criteria for the particle size, thus performing a quality-based selection.

2. Materials and Methods

2.1. Materials

Meloxicam (MLX), magnesium stearate (MgSt), sodium hydroxide, hydrochloric acid, ethanol, and acetone were purchased from Sigma Aldrich (St. Louis, MO, USA). Vivapur 200 microcrystalline cellulose (MCC) was purchased from JRS Pharma (Rosenberg, Germany).

2.2. Preparation of different particle size fractions from MLX

Different particle size fractions were produced from the initial MLX using crystallization methods for particle size analysis. The denotation of these groups contained the measured, rounded D50 values in the subscript. If any crystallization process was applied, the solvent was named in the superscript. The denotations and the differences between the particle size groups were summarized in ***Table 1***.

The applied technique for the particle size enlargement of $MLX_{25\mu m}$ was based on the publication of crystallization using a slow cooling method by Bolourchian et al. [31]. Accordingly, 1 g of $MLX_{25\mu m}$ was placed in a crystallization dish and dissolved in acetone at 50°C using 100 rpm stirring. The applied $MLX_{25\mu m}$ concentration was 0.45 w/v%. The solution was kept overnight at room temperature to evaporate the applied solvent. The obtained crystals were gathered in a glass sample holder and stored at room temperature. When ethanol solvent was applied, the aforementioned slow cooling method was used and the $MLX_{25\mu m}$ concentration was set to 0.16 w/v%

Crystallization was also applied to produce a fine particle size fraction from $MLX_{25\mu m}$. Based on the patent of Coppi et al., 1g of $MLX_{25\mu m}$ was placed in a beaker and dissolved in sodium hydroxide solution (1 equivalent of NaOH with respect to $MLX_{25\mu m}$, water/ $MLX_{25\mu m}$ ratio was set to 30) at 45°C, using 100 rpm stirring. When a clear solution was obtained, the pH was adjusted to 4 with hydrochloric acid. The obtained suspension was kept at 45°C for 60 minutes [32]. After a cooling step, crystals were filtered, washed with distilled water, and dried. The obtained crystalline fraction was gathered and stored the same as mentioned. The applied crystallization methods were reproduced in both cases to collect sufficient amount of crystalline samples.

Table 1. *The denotations and the attributes of different particle size samples of MLX*

Denotation of the different particle size samples	Applied solvent for crystallization	Measured particle size range	Measured D50 value
$MLX_{5\mu m}^{NaOH}$	NaOH/HCl	<10 µm	5.490 µm
$MLX_{25\mu m}$	-	<50 µm	25.048 µm
$MLX_{176\mu m}^{Acetone}$	Acetone	<440 µm	176.113 µm
$MLX_{303\mu m}^{EtOH}$	Ethanol	<472 µm	303.148 µm

2.3. Particle size analysis of the prepared MLX crystals

The PSDs of different particle size samples (***Table 1.)*** were determined by laser diffraction-based method executed on Malvern Mastersizer 2000 (Malvern Panalytical Ltd., UK) with Scirocco 2000 (Malvern Panalytical Ltd., UK) sample dispersion unit. The instrumentation allows particle-in-gas particle size analysis.

1g of crystalline sample was placed on the sample tray of the dispersion unit manually. Due to the vibration of the tray, the sample was fed into a sieve with bearings for controlled sample flow and to break the loose agglomerates. The sample flow and the dispersion were provided by compressed air. The applied standard operation procedure parameters were the followings: vibrational feed rate was set to 40%, dispersive air pressure was set to 1 bar, and measurement time was 30 seconds. The applied theory of particle size analysis is based on the Mie theory. The measurement range of this instrument takes from 100 nm to 2 mm.

2.4. Preparation of the tablets

In the first experiment, tablets were produced to train, validate, and test the pattern recognition neural network, which executed the particle size-based classification task. These tablets were also crucial in the development phase of the algorithms for particle size analysis using UV/VIS images, especially identifying the API with different particle sizes. To test the capabilities of the developed system in finer and larger particle size ranges than the target, powder blends from the four different particle size samples (**Table 1.**) and a mixture was prepared from $MLX_{25\mu m}$ and $MLX_{5\mu m}^{NaOH}$ and used as APIs. The authors determined the PSD of $MLX_{25\mu m}$ as target.

After weighing the appropriate amount from the different particle size samples of MLX (**Table 1.**), 10.5 g powder blends with 2.5 m/m% API content were prepared using MCC as excipient (**Table 2.**). The API content was determined based on the commercially available MLX-containing tablets. In the first experiment, no MgSt addition was to avoid other interfering parameters in the development phase of the particle size analysis methods. The lubrication was provided between the tableting of the different particle size groups.

To maintain the integrity of the different particle size samples and to avoid the breaking of the prepared crystals, the homogenization step was executed by manual blending for 10 minutes. From each powder mixture, 25 tablets were produced one by one on a Dott Bonapace CPR-6 (Dott Bonapace, Italy) eccentric tablet press, equipped with a single concave punch using 10 ± 1 kN compression force. Biconvex tablets were obtained with a diameter of 14 mm, the weight of the tablets was 400 ± 15 mg, and the content of the applied API was 10 ± 0.5 mg per tablet.

Table 2. *The attributes of the prepared tablets for the particle size analysis and particle size-based classification*

Number of the prepared tablets	Prepared different particle size samples	Applied excipient	Compression force	API content
1-25.	$MLX_{5\mu m}^{NaOH}$	MCC	10 kN	2.5 m/m%
26-50.	$MLX_{25\mu m}$	MCC	10 kN	2.5 m/m%
51-75.	$MLX_{176\mu m}^{Acetone}$	MCC	10 kN	2.5 m/m%
76-100.	$MLX_{303\mu m}^{EtOH}$	MCC	10 kN	2.5 m/m%
101-125.	$MLX_{5\mu m}^{NaOH}$ $MLX_{25\mu m}$	MCC	10 kN	0.5 m/m% 1.5 m/m%

The further experiment aimed to test the capabilities of the developed machine vision system to identify changes in the particle size from $MLX_{25\mu m}$. The tableting was executed in automatic mode on the same instrumentation supplemented with a feed frame. Two blends containing the target and finer or larger particle size fractions ensure the changes in the system. After weighing the components, 22 g of powder blends were prepared using the homogenization method. The compositions of the applied powder blends are presented in **Table 3.** In this experiment, MgSt was also added to the powder blends to determine its effect on the classification and particle size analysis both in UV and VIS images. After 5.5g of powder blend containing $MLX_{25\mu m}$ was fed into the feed frame of the tablet press, the tableting process started. Defined amounts of the following blends were layered in a specific order (**Table 3.**) with time shifts to ensure the occurrence of tablets containing the approved particle size of the API.

Table 3. *The order and attributes of the prepared powder blends for the automatic tableting experiment*

Order of the applied blends	Particle size sample	Applied excipients	Compression force	API content	Weight of the powder blend per layer
1.	$MLX_{25\mu m}$	MgSt (1%) MCC	10 kN	2.5 m/m%	5.5g
2.	$MLX_{5\mu m}^{NaOH}$ $MLX_{25\mu m}$	MgSt (1%) MCC	10 kN	0.5 m/m% 1.5 m/m%	22g
3.	$MLX_{25\mu m}$	MgSt (1%) MCC	10 kN	2.5 m/m%	5.5g
4.	$MLX_{176\ \mu m}^{Acetone}$ $MLX_{25\mu m}$	MgSt (1%) MCC	10 kN	0.5 m/m% 1.5 m/m%	22g
5.	$MLX_{25\mu m}$	MgSt (1%) MCC	10 kN	2.5 m/m%	11g

2.5. Image acquisition

Images were acquired using a Canon 650D (Canon, Japan) DSLR (digital single-lens reflex) camera and Canon EFS 18-55 macro lens (Canon, Japan) mounted with a reversing ring. The camera was connected to a computer with a USB 3.0 interface. UV images were taken using a ring light containing one row of UV light-emitting diodes emitting in the 380-395 nm range (Apokromat Ltd, Hungary), and VIS images were taken using a ring light containing three rows of white, light-emitting diodes. Images were taken from both sides of the prepared tablets. The resolution of the acquired images was 3456×5184 pixels. The layout of the image acquisition, which can be mounted on a conveyor belt, was designed in-house. This was analogous, as shown in the previous publication of the authors [33]. The calibration of the system was executed with QPCard 101 v3 millimeter reference scale (Argraph Corp., NJ, USA). After the calibration of the system, the size of a pixel was 4.2 µm. For image resizing, a sophisticated mathematical approach, Lanczos kernel was applied, which provided an opportunity to reduce a pixel size to 2.2 µm.

2.6. Particle size-based classification and particle size analysis with the developed machine vision system

2.6.1. Particle size-based classification of the prepared tablets

Two image processing algorithms were developed for UV and VIS images (**Figure 1.**) in Matlab 2020a (Mathworks, Natick, MA, USA). Particle size-based classification tasks were executed using Pattern Recognition Neural Network from Pattern Recognition and Machine Learning Toolbox (Mathworks, Natick, MA, USA).

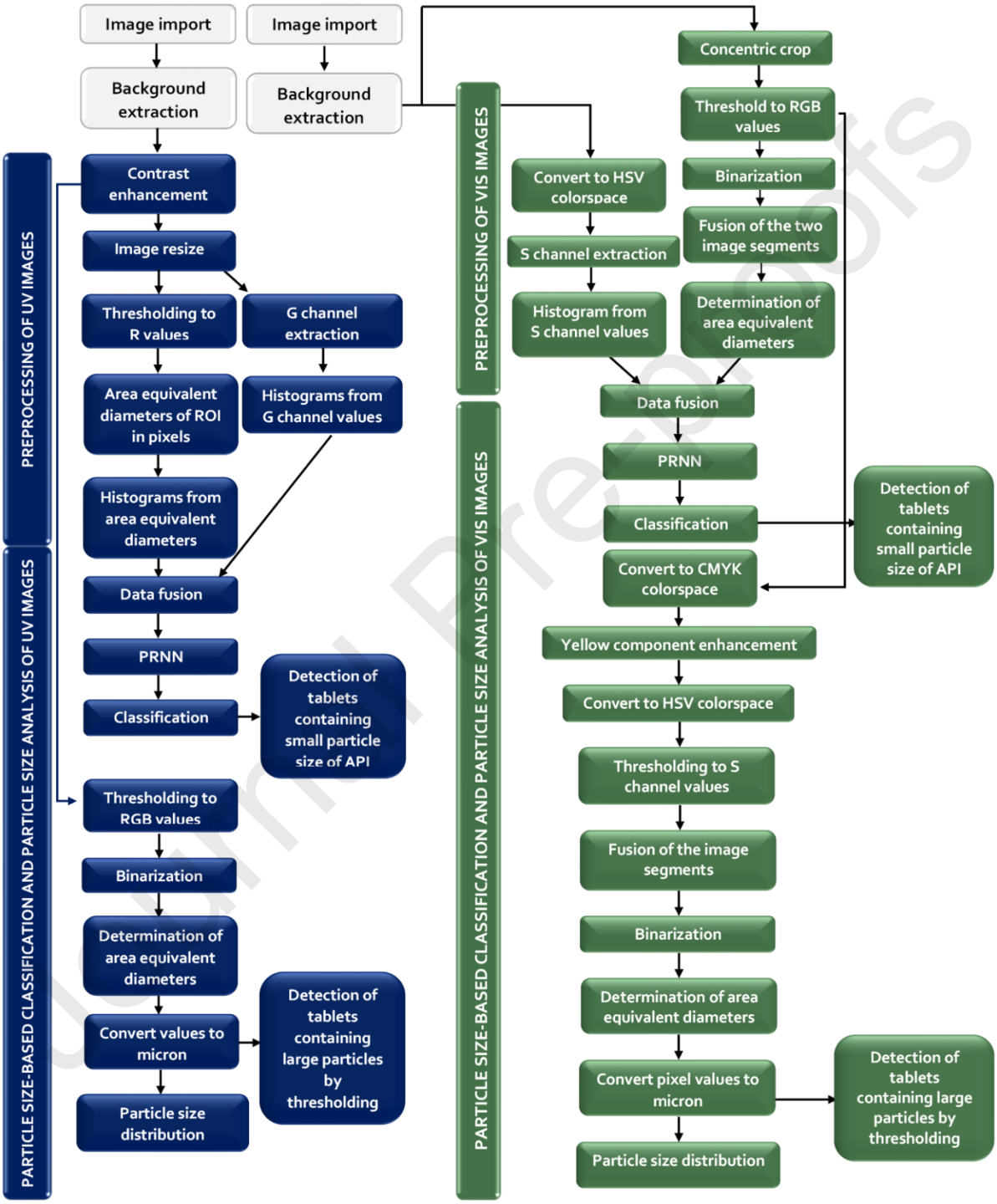

Figure 1. *UV and VIS image processing algorithms for classification and particle size analysis*

After the image importing and the background extraction steps, UV images were resized to 20% of the original size. The resizing allowed the reduction of the image processing duration and the time consumption of the classification. For the classification task, the determination of the exact R, G, and B threshold values were not necessary because only the extraction of the distinguishable features and the regions of interest (ROIs) were required. Identifying ROIs was achievable using more permissive thresholds for only one channel from the applied colorspace. After the thresholding step, the obtained logical values were used to generate binary images. Then area equivalent diameters of the ROIs were calculated. Histograms were created from these values and used as input for pattern recognition neural network after normalization.

In the applied network, 50 neurons were applied in one hidden layer with a saturating linear transfer function, and 5 neurons were applied in the output layer with softmax transfer function. The pattern recognition neural network was trained using scaled conjugate gradient backpropagation. The end of the training was determined by reaching the appropriate number of validation checks. The training sample set contained 70%, the validation and the test set contained 15%-15% of the samples prepared in the first tableting experiment. Classes were determined according to the prepared different particle size samples and marked with Boolean operators in a target matrix. For evaluating the performance of the network, cross-entropy and mean squared error were calculated. Neural networks were also trained using the resized images and only two classes in the target matrix for approval or rejection of the tablets.

A similar method was applied to determine area equivalent diameters of ROIs based on VIS images as for UV images. The main difference is in the concentrical segmentation of the tablet to the edge and the central regions. Due to the shape and the applied compression force the prepared tablets were changed in the saturation of color from the center to the edge. The changes in the color saturation were also observable, mainly when $MLX_{25\mu m}$ and $MLX_{5\mu m}^{NaOH}$ groups were applied. $MLX_{5\mu m}^{NaOH}$ caused a more saturated color on the surface of the tablets than $MLX_{25\mu m}$. Thus, after the conversion from RGB to HSV colorspace, the S channel histograms were applied. In the last step of VIS image processing, histograms of the S channel and the area equivalent diameter values were fused to create the input dataset for the pattern recognition neural network. The applied neural network structure was the same as used in the classification of UV images.

The developed algorithms also contained a simple approval limit for the particle size of the API. This made easily identifiable even one large MLX particle on UV and VIS images, and it

supported the results of the pattern recognition neural networks. In that case, precise thresholding was applied for the API. Then the sizes of MLX particles were determined based on section 2.6.2. The upper approval limit (100 μm) was determined based on the obtained PSD of $MLX_{25\mu m}$.

2.6.2. Particle size analysis of tablets

The algorithms for the particle size analysis using UV and VIS images are shown in **Figure 1.** The appropriate threshold values for R, G, and B channels were applied to identify the MLX particles on UV images. Binary images were created from the obtained logical values. The area equivalent diameters were determined in pixels, and then these values were converted to micron. The PSDs, D10, D50, D90 values, and span were calculated in the last step.

A complex algorithm had to be developed for particle size analysis using VIS images. The first step was the concentric crop of the images. The image segments were converted to CMYK colorspace. In that colorspace, the yellow component corresponds to one channel. Thus, the enhancement of MLX particles can be executed. The image segments were converted to HSV colorspace, and thresholding to S channel values was executed. Binary images were created with the fusion of the preprocessed image segments. The determination of the PSDs and the statistical values were obtained as in the analysis of UV images.

2.7. Statistical comparison of the measured and the predicted particle size distributions

The measured PSDs were compared to the predicted PSDs using the nonparametric, two-sample Kolmogorov-Smirnov test. The null hypothesis of the test was the measured and the predicted PSDs came from the same distribution. The null hypothesis was rejected or approved at 5% significance level. In this work, complex, bimodal PSDs were obtained, thus Wasserstein distance was also calculated for comparison.

3. RESULTS AND DISCUSSION

3.1. Particle size analysis of the prepared MLX crystals

The acquired UV images taken from the different particle size samples are shown in **Figure 2.** Based on the obtained statistical values of the measured PSDs the different particle size fractions of MLX were successfully prepared. As Boluruchian *et al.* mentioned the agglomerates cannot be disaggregated with 1 minute sonication [31]; this affected $MLX_{176\,\mu m}^{Acetone}$, and $MLX_{303\,\mu m}^{EtOH}$ groups. The occurring aggregates also caused differences between the measured statistical values in the presented and the mentioned publication. However, the utilization of the prepared crystals and agglomerates are suitable for the goal of the authors to detect and classify defective tablets in the context of particle size, to determine the particle size of $MLX_{25\mu m}$ and particle domain size of $MLX_{176\,\mu m}^{Acetone}$ and $MLX_{303\,\mu m}^{EtOh}$, and to identify tablets containing $MLX_{5\mu m}^{NaOH}$.

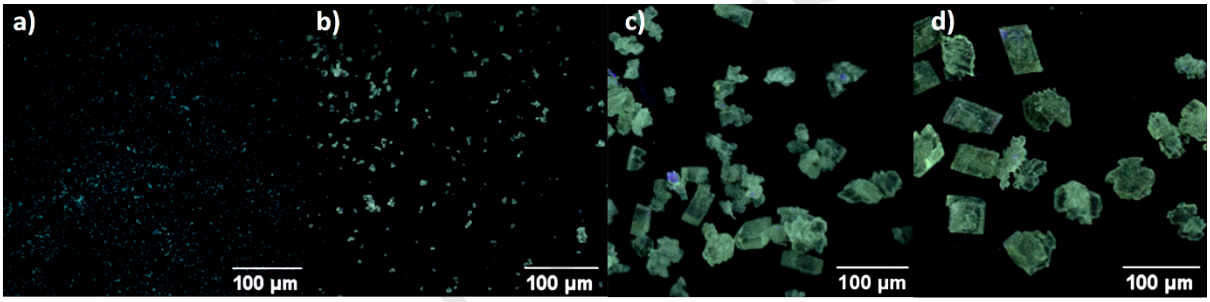

Figure 2. *The acquired UV images from the different particle size groups of MLX crystals (a)* $MLX_{5\mu m}^{NaOH}$*, b)* $MLX_{25\mu m}$*, c)* $MLX_{176\,\mu m}^{Acetone}$*, d)* $MLX_{303\,\mu m}^{EtOH}$*)*

3.2. Acquired images from the prepared tablets containing different particle sizes of MLX

The acquired images from the prepared tablets for the classification and the particle size analysis were shown in **Figure 3.**

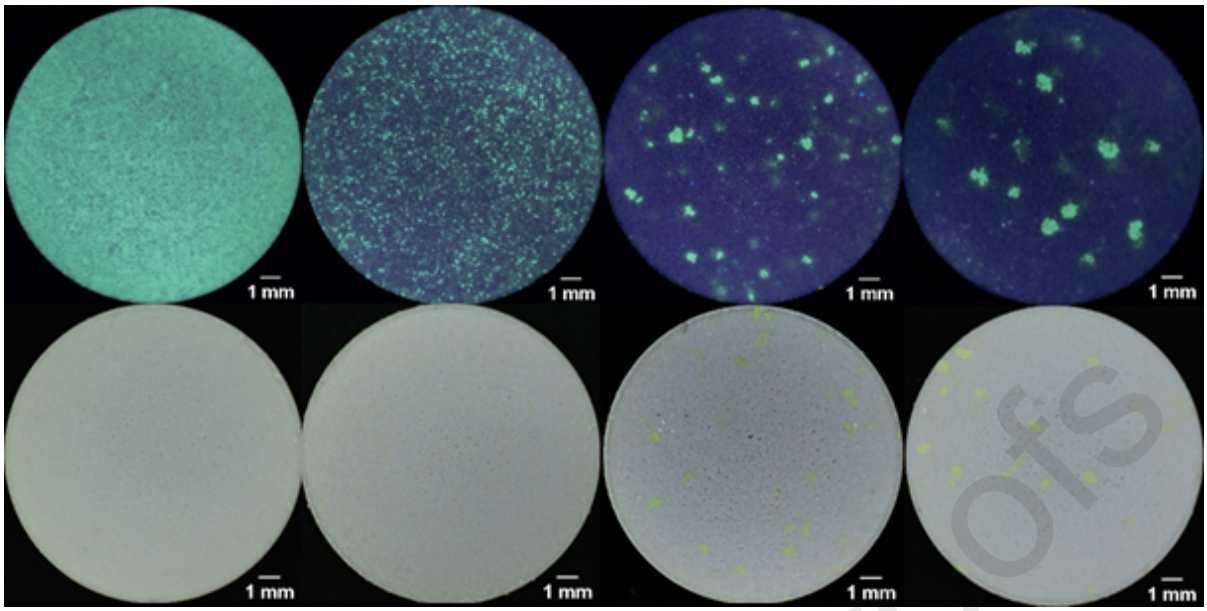

Figure 3. *The acquired images from the tablets containing different particle sizes of MLX (left to right: a tablet containing* $MLX_{5\mu m}^{NaOH}$, $MLX_{25\mu m}$, $MLX_{176\,\mu m}^{Acetone}$, *and* $MLX_{303\,\mu m}^{EtOH}$). *The first row of the images was taken using UV illumination, the second row of the images was taken using VIS illumination of the same tablets.*

Based on **Figure 3,** the API particles of the different particle size groups were more distinguishable using UV illumination. On the VIS images, API particles of $MLX_{303\,\mu m}^{EtOH}$, and $MLX_{176\,\mu m}^{Acetone}$ were distinguishable to the naked eyes. Individual $MLX_{5\mu m}^{NaOH}$ particles were not distinguishable at the API content of 2.5 m/m%, making the particle size analysis not feasible in that group. The differences in particle size were not observable between the $MLX_{5\mu m}^{NaOH}$ and $MLX_{25\mu m}$ groups using VIS illumination; only a slight color change differentiated the two groups. However, these observations enabled the qualitative analysis of the tablets under UV and VIS illumination in the case of the $MLX_{5\mu m}^{NaOH}$ group.

The acquired images from the application experiment of the machine vision system are shown in **Figure 4.**

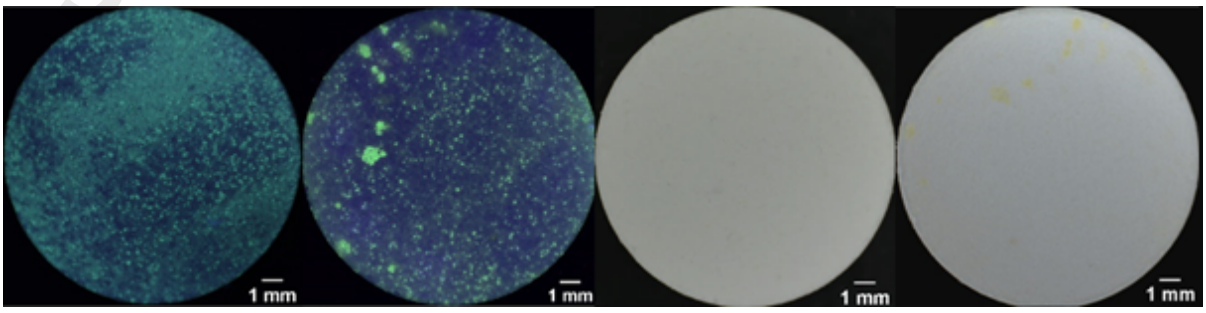

Figure 4. *The acquired images from the tablets prepared in automatic tableting mode (images from left to right:* $MLX_{5\mu m}^{NaOH}$ *+* $MLX_{25\mu m}$*,* $MLX_{176\,\mu m}^{Acetone}$ *+* $MLX_{25\mu m}$ *containing tablets under UV and VIS illumination)*

The $MLX_{5\mu m}^{NaOH}$ *+* $MLX_{25\mu m}$ containing tablets were more identifiable with UV images than with VIS images. In the case of $MLX_{176\,\mu m}^{Acetone}$ *+* $MLX_{25\mu m}$ containing tablets, the appearance was similar to the $MLX_{25\mu m}$ group with the aleatory occurrence of large $MLX_{176\,\mu m}^{Acetone}$ particles. However, few $MLX_{176\,\mu m}^{Acetone}$ particles were on the surface of the presented tablet (**Figure 4**.), there could be high variability in the occurrence of these large particles.

3.3. Particle size-based classification of the prepared tablets

The particle size-based classification was executed with the developed image processing algorithms and pattern recognition neural networks (**Figure 1.**) based on the images taken from the prepared tablets using the two different illuminations (**Figure 3.**).

The cross-entropy and mean squared error values for the training, validation, and test set were summarized in **Table 4.** and the confusion matrices obtained with the developed image processing were shown in **Figure 5.** for the different illuminations.

Table 4*. Cross-entropy and error percentage values of the training, validation, and test set for UV and VIS images taken from both sides of the tablets*

Image preprocessing	Image type	Set	Percentage of correct classification	Percentage of incorrect classification	Cross-entropy	MSE
Image resize (5 classes)	VIS	Training	93.53%	6.47%	$3.3*10^{-2}$	$4.7*10^{-3}$
		Validation	90.00%	10.00%	$3.4*10^{-2}$	$3.5*10^{-2}$
		Test	90.00%	10.00%	$3.6*10^{-2}$	$3.7*10^{-2}$
Image resize (5 classes)	UV	Training	99.41%	0.59%	$9.2*10^{-4}$	$6.8*10^{-4}$
		Validation	97.5%	2.50%	$4.5*10^{-2}$	$7.8*10^{-3}$
		Test	100%	0%	$6.5*10^{-5}$	$3.5*10^{-7}$
Image resize (2 classes)	VIS	Training	99.41%	0.59%	$4.5*10^{-3}$	$4.7*10^{-3}$
		Validation	97.50%	2.50%	$1.3*10^{-3}$	$1.3*10^{-1}$
		Test	95.00%	5.00%	$1.8*10^{-2}$	$2.1*10^{-2}$
Image resize (2	UV	Training	100%	0%	$6.2*10^{-10}$	$4.2*10^{-5}$

classes)		Validation	100%	0%	$4.7*10^{-10}$	$3.5*10^{-5}$
		Test	100%	0%	$6.0*10^{-10}$	$2.8*10^{-5}$
Image processing algorithm (5 classes)	VIS	Training	97.06%	2.94%	$5.0*10^{-2}$	$1.0*10^{-2}$
		Validation	100.0%	0.00%	$3.0*10^{-2}$	$1.1*10^{-2}$
		Test	100.0%	0.00%	$4.1*10^{-2}$	$1.0*10^{-2}$
Image processing algorithm (5 classes)	UV	Training	99.41%	0.59%	$2.1*10^{-2}$	$1.0*10^{-2}$
		Validation	100.0%	0.00%	$2.0*10^{-2}$	$1.0*10^{-2}$
		Test	97.50%	2.50%	$2.0*10^{-2}$	$1.1*10^{-2}$
Image processing algorithm (2 classes)	VIS	Training	97.75%	2.35%	$2.6*10^{-2}$	$2.6*10^{-2}$
		Validation	97.50%	2.50%	$3.4*10^{-2}$	$3.9*10^{-2}$
		Test	95.00%	5.00%	$1.0*10^{-1}$	$5.0*10^{-1}$
Image processing algorithm (2 classes)	UV	Training	100%	0%	$3.46*10^{-5}$	$6.34*10^{-4}$
		Validation	100%	0%	$1.9*10^{-1}$	$2.5*10^{-1}$
		Test	100%	0%	$1.9*10^{-1}$	$2.5*10^{-1}$

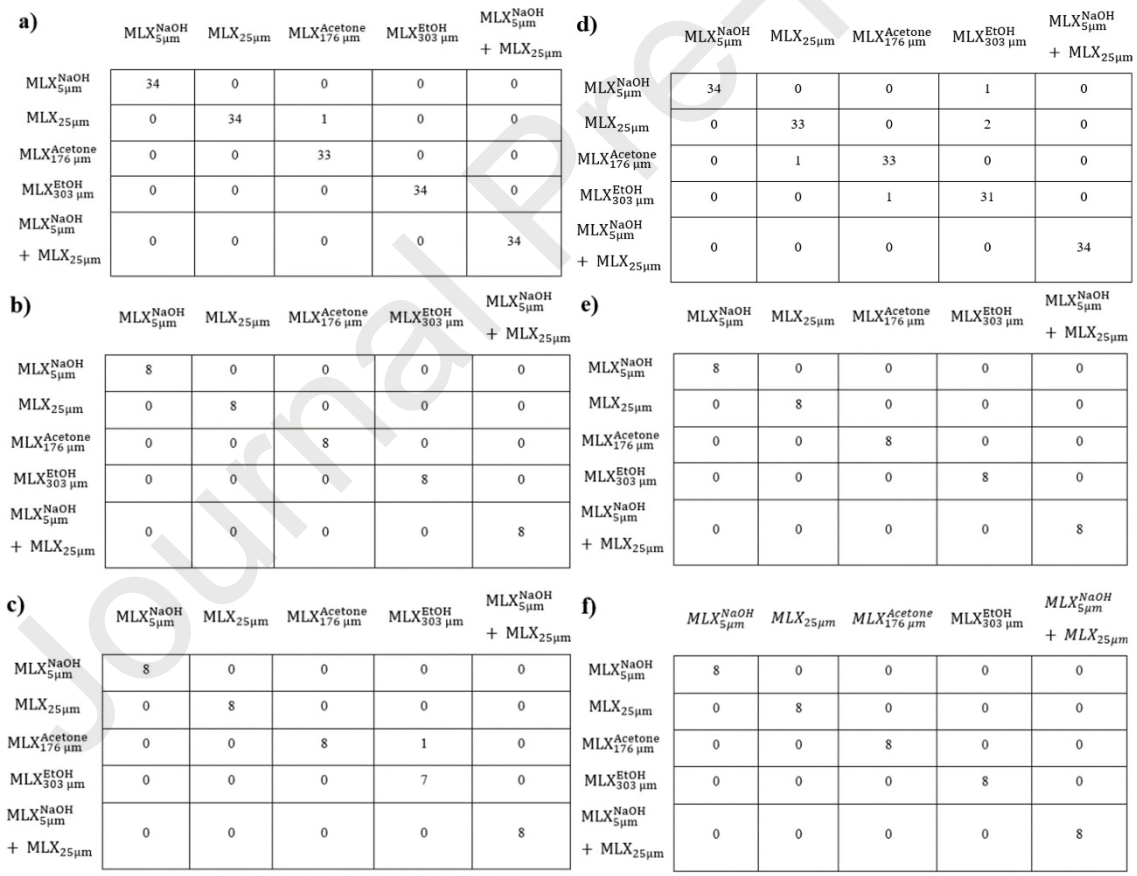

Figure 5. *Confusion matrices of the pattern recognition neural network-based classification using image processing algorithms and five classes (a) training, b) validation, c) test set for UV images, d) training, e) validation and f) test set for VIS images)*

According to **Table 4.** binary classification can be executed with or without preprocessing of the resized UV or VIS images.

When five classes were applied regarding the different particle size samples, satisfactory results were achieved using UV images with or without the preprocessing algorithm. However, when VIS images were used as inputs, better results were achieved with the developed image processing algorithm. Due to the applied image processing algorithms, neural networks used a significantly smaller matrix as input dataset containing the appropriate information. This related to the duration of the classification, which might be a significant advantage.

In **Figure 5.** the obtained confusion matrices were presented using five classes and image processing. In the case of the training set of UV images, only one tablet side, thus a tablet was misclassified to $MLX_{176\,\mu m}^{Acetone}$ instead of $MLX_{25\mu m}$ group. From the validation sample set one was also misclassified to $MLX_{303\,\mu m}^{EtOH}$instead of $MLX_{176\,\mu m}^{Acetone}$ group. The other samples from all the sample sets were classified correctly.

In the case of VIS images, five samples were misclassified. The most considerable are three samples from the $MLX_{303\,\mu m}^{EtOH}$ group. The samples of the validation and the test sample set were classified correctly.

3.4. Particle size analysis of the prepared tablets containing different particle sizes of MLX

After the prepared tablets were classified, the particle size analysis was executed. The obtained PSDs and the statistical values were shown in **Figure 6.** and **Table 5.** for UV and VIS images. These distributions and statistical values were obtained as a summary from all the images taken from the prepared tablets. The reference distributions and statistical values were obtained from the initial crystals of different particle size samples of MLX using an off-line laser diffraction-based method.

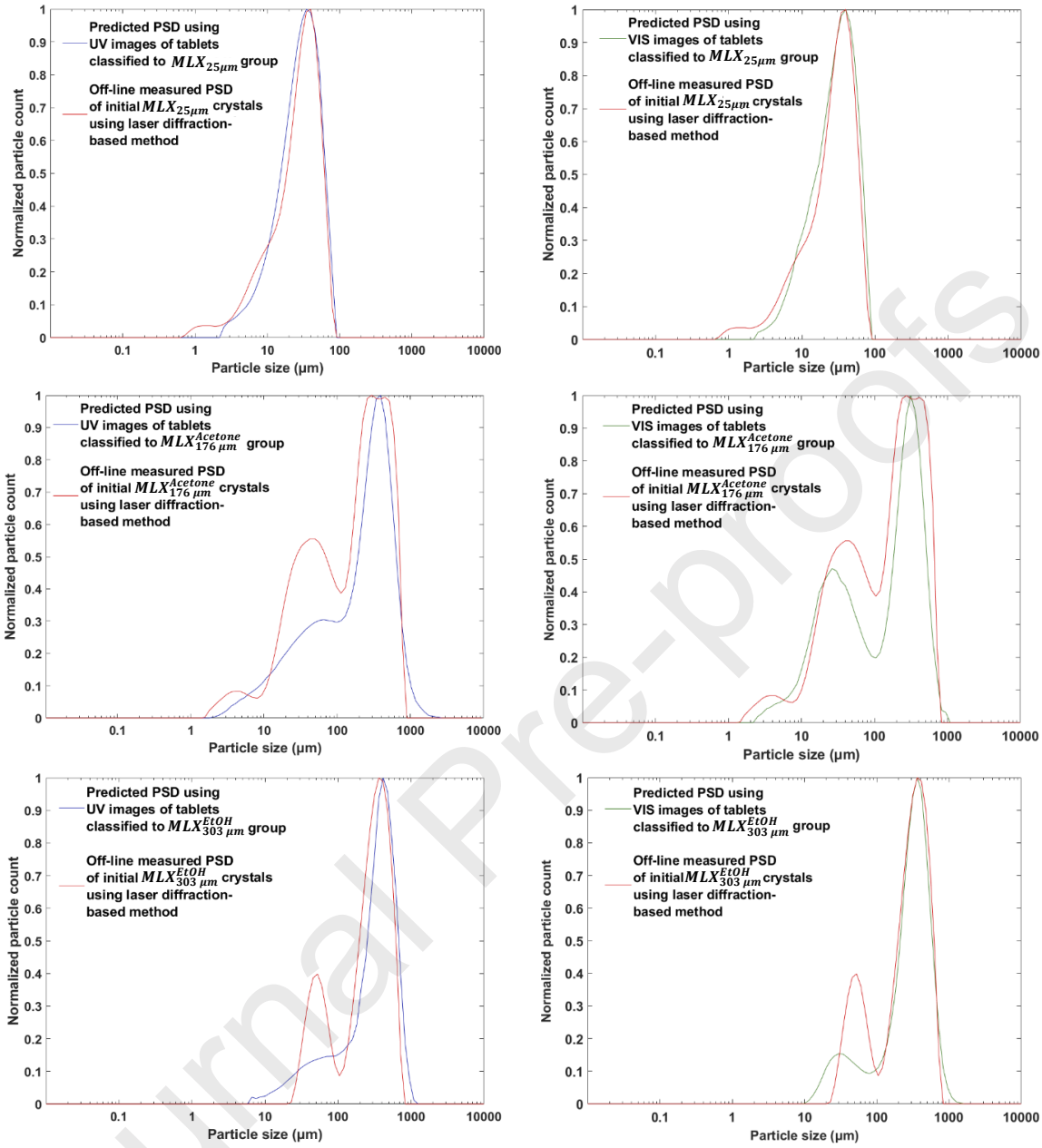

Figure 6. *The measured and the obtained PSDs of MLX tablets supported by digital UV/VIS imaging and image processing coupled with pattern recognition neural network (left column: results based on UV images, right column: results based on VIS images)*

Table 5. *The calculated statistical values of PSDs based on the standard laser diffraction method and the acquired UV and VIS images of all tablets containing different particle size groups of the API*

Statistical values of PSDs measured from the initial crystalline API using off-line laser diffraction-based method				
MLX group	***D50 (µm)***	***D10 (µm)***	***D90 (µm)***	***Span***
$MLX_{5\mu m}^{NaOH}$	5.490	2.591	10.0310	1.3526
$MLX_{25\mu m}$	25.048	6.093	47.9362	1.6750
$MLX_{176\ \mu m}^{Acetone}$	176.113	16.3702	439.9254	2.4053
$MLX_{303\ \mu m}^{EtOH}$	303.148	41.7485	471.8890	1.4196

Statistical values of PSDs predicted from tablets using UV images				
MLX group	***D50 (µm)***	***D10 (µm)***	***D90 (µm)***	***Span***
$MLX_{5\mu m}^{NaOH}$	100% of the samples were detected by pattern recognition neural network			
$MLX_{25\mu m}$	24.14	8.27	48.47	1.67
$MLX_{176\ \mu m}^{Acetone}$	192.43	16.75	476.33	2.39
$MLX_{303\ \mu m}^{EtOH}$	279.79	39.50	514.92	1.70

Statistical values of PSDs predicted from tablets using VIS images				
MLX group	***D50 (µm)***	***D10 (µm)***	***D90 (µm)***	***Span***
$MLX_{5\mu m}^{NaOH}$	98.00% of the samples were detected by pattern recognition neural network			
$MLX_{25\mu m}$	24.29	7.94	48.18	1.66
$MLX_{176\ \mu m}^{Acetone}$	133.43	12.59	369.57	2.68
$MLX_{303\ \mu m}^{EtOH}$	249.42	33.87	469.55	1.72

The fine particle size of $MLX_{5\mu m}^{NaOH}$ made the particle size analysis not feasible because the individual particles were not distinguishable with the applied resolution of the images. In other cases, the calculated distributions were similar to the measured distributions. Between the measured and the predicted PSDs differences could occur because the agglomerates or the crystals can break apart and deform during the homogenization or the tableting steps of the process.

Considering the statistical values in **Table 5.**, a slight difference can be observed between the measured and the predicted D50, D10, D90, and span values in the $MLX_{25\mu m}$ group. These deviations are substantially higher in respect of $MLX_{176\ \mu m}^{Acetone}$ and $MLX_{303\ \mu m}^{EtOH}$ groups.

Table 6. *The results of Kolmogorov-Smirnov tests and the Wasserstein distances between the off-line measured PSDs of the initial crystals of the API and the predicted PSDs of all the tablets of different particle size groups using UV and VIS images*

MLX group	***Image type***	***p value from Kolmogorov-Smirnov test***	***Wasserstein distance from the measured distribution***
$MLX_{25\mu m}$	UV	0.6828	0.0145
	VIS	0.6828	0.0147
$MLX^{Acetone}_{176\ \mu m}$	UV	0.1930	0.0535
	VIS	0.3499	0.0480
$MLX^{EtOH}_{303\ \mu m}$	UV	0.3499	0.0247
	VIS	0.5626	0.0233

According to the p values of two-sample Kolmogorov-Smirnov tests, the H0 was not rejected for any MLX groups. From the comparison of the measured and the predicted PSDs shown in **Figure 6.** the prediction of the $MLX_{25\mu m}$ group showed higher similarity to the measured distribution. This assertion was supported by high p values of the Kolmogorov-Smirnov test and the lowest Wasserstein distance values using UV and VIS images (**Table 6.**). In the case of $MLX^{Acetone}_{176\ \mu m}$ and $MLX^{EtOH}_{303\ \mu m}$ groups, the obtained results using showed similar distributions to the measured PSDs. However, the Wasserstein distance values were higher than for the $MLX_{25\mu m}$ group.

Using the developed image processing algorithms for UV and VIS images, the determination of PSD of $MLX_{25\mu m}$ group was possible, which was also supported by statistical comparisons. However, only a domain size can be accurately determined in the context of the $MLX^{Acetone}_{176\ \mu m}$ and $MLX^{EtOH}_{303\ \mu m}$ groups. Important to mention that the machine vision system can collect information from every individual tablet, which can monitor these unexpected changes during the production process.

3.5. Application of the developed machine vision system for particle size-based classification and particle size distribution determination in intact tablets

An automated tableting-based experiment was executed to model an API batch change or segregation. The presented work tended to show the changes in particle sizes in the prepared tablets, being above or below the desired particle size. The created two scenarios were presented in **Figure 7. a)** and **b)**. These justified the necessity of applying the pattern recognition-based classification and the extended version of thresholding to the desired value.

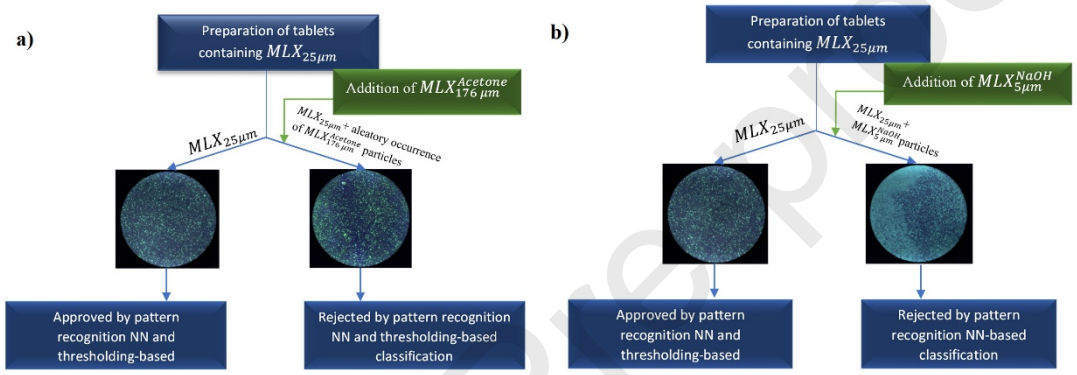

***Figure** 7. The two scenarios, which can occur in automatic tableting in the context of batch changes of different particle size fractions, when (a) adding $MLX_{176\,\mu m}^{Acetone}$+ $MLX_{25\mu m}$, and b) adding $MLX_{5\mu m}^{NaOH}$+ $MLX_{25\mu m}$ to the initial $MLX_{25\mu m}$powder mixture)*

The image processing algorithms and pattern recognition neural networks were the same as used for assessing the tablets prepared in the first tableting experiment. The approval limit approach played a considerable role in the occurring scenarios, especially when $MLX_{176\,\mu m}^{Acetone}$ was presented in the initial $MLX_{25\mu m}$ powder mixture.

In the automatic tableting mode, 155 tablets were prepared (**Table 2.**). 53 and 102 tablets were approved and rejected, respectively. 51 of the rejected tablets contained the $MLX_{5\mu m}^{NaOH}$ + $ML X_{25\mu m}$, and 51 contained the $MLX_{176\,\mu m}^{Acetone}$+ $MLX_{25\mu m}$ mixture. The tablets containing the $ML X_{25\mu m}$ fraction got an approval value which equals one using Boolean operators. All the other samples were rejected and got zero values. The summarized results for the approval of the samples are shown in **Figure 8. a)** and **b)** for UV and VIS images.

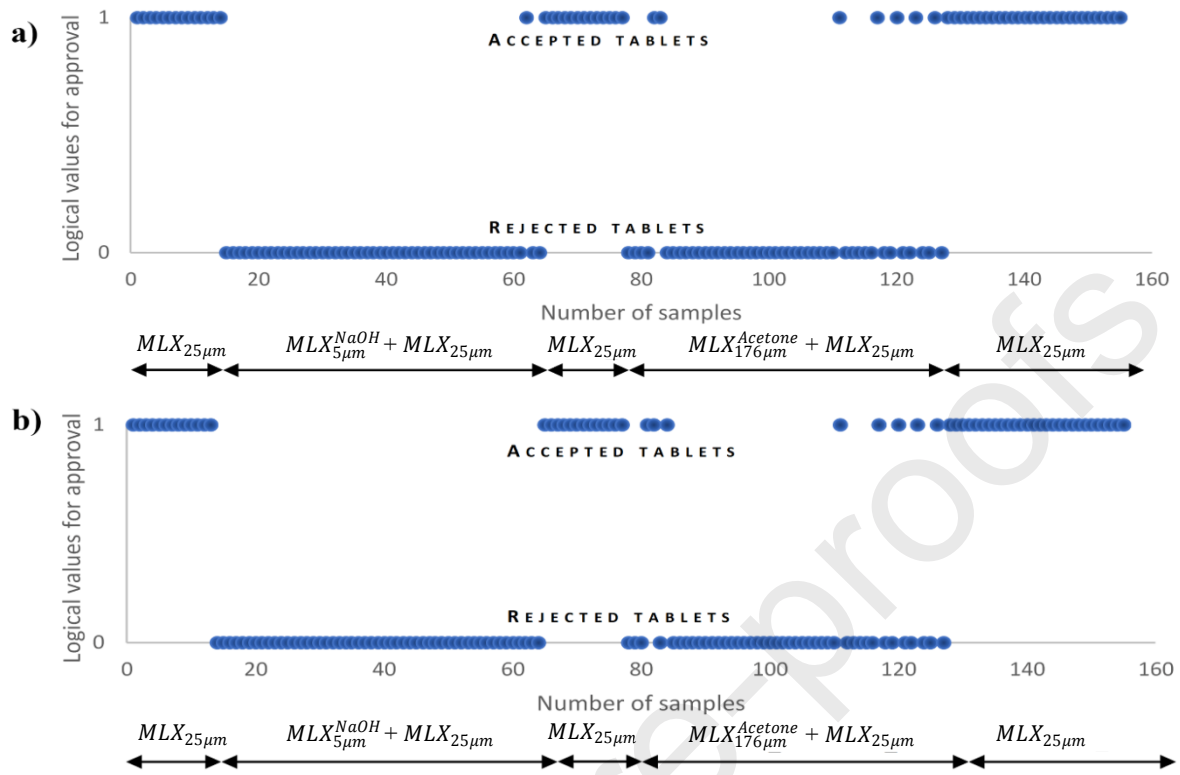

Figure 8. *The summarized approval results of the continuously prepared tablets selected by classification using pattern recognition neural network and thresholding-based algorithms (a) results based on UV images and b) VIS images of the prepared tablets)*

According to UV and VIS images, rejected tablets in the sample range of 1-65 were classified to $MLX_{5\mu m}^{NaOH}$+ $MLX_{25\mu m}$ group by pattern recognition neural networks. From sample range of 66-155 the approvable tablets were classified into the group of $MLX_{25\mu m}$ and the thresholding algorithms detected the occurrence of $MLX_{176\,\mu m}^{Acetone}$ particles. If the percentage of incorrect classification is considered from the summarized results of approval values, 2% was obtained in the case of UV and 1.3% was obtained for VIS illuminated images.

In **Figure 9.** the resulted PSDs of the digital UV/VIS imaging-based particle size analysis were presented. In the case of the target $MLX_{25\mu m}$ group the PSDs were similar to the measured distributions based on the statistical comparisons (**Table 7.)**

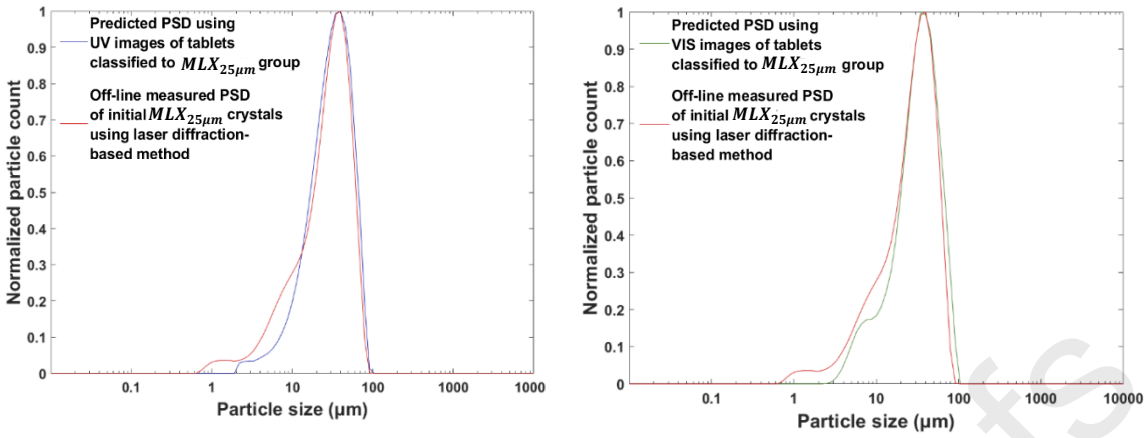

Figure 9. *The off-line measured PSD of initial crystals and the predicted PSDs of all accepted tablets containing* $MLX_{25\mu m}$ *supported by digital UV/VIS imaging and image processing (results based on UV images (left), right and results based on VIS images (right))*

Table 7. *The results of particle size analysis by digital UV/VIS imaging-based machine vision system and the results of the statistical analysis of the obtained PSDs*

Statistical values of PSDs predicted from tablets using VIS images						
Class	***D50 (μm)***	***D10 (μm)***	***D90 (μm)***	***Span***	***p value***	***Wasserstein distance***
$MLX_{25\mu m}$	26.67	8.51	50.92	1.60	0.6828	0.0094
$MLX_{5\mu m}^{NaOH}+$ $MLX_{25\mu m}$	Detected by classification using pattern recognition neural network					
$MLX_{176\ \mu m}^{Acetone}+$ $MLX_{25\mu m}$	38.68	12.11	226.19	5.53	0.6766	0.0393
Statistical values of PSDs predicted from tablets using UV images						
Class	***D50 (μm)***	***D10 (μm)***	***D90 (μm)***	***Span***	***p value***	***Wasserstein distance***
$MLX_{25\mu m}$	25.34	9.60	48.05	1.52	0.8972	0.0162
$MLX_{5\mu m}^{NaOH}+$ $MLX_{25\mu m}$	Detected by classification using pattern recognition neural network					
$MLX_{176\ \mu m}^{Acetone}+$ $MLX_{25\mu m}$	40.87	16.01	187.93	4.21	0.6828	0.0386

The changes in particle size from the target have a significant impact on the quality, safety and efficiency of the tablets. The *in vitro* dissolution rate significantly increases, and the dissolution profile can be modified with the application of fine API particles. The large particle significantly slower the dissolution of the product. The particle size also affects the flowability and compressibility, thus fine particles have the worst performance.

The applied MLX concentration in this work was considered adequate but relatively low. The developed thresholding-based method can be applied up to the API concentration when the particles are not overlapping. Consequently, the developed model should be applied to much higher MLX concentrations without any modifications. Although, when the particles overlap to a large extent, advanced methods should be applied for particle identification.

It is worth mentioning that the developed method needs to be adjusted to the API UV activity and color in VIS, the applied particle size, the API content, the applied excipients and the resolution of the images. A single tablet image can be enough to determine if the particle size analysis works. Another outstanding feature is that the algorithms do not depend on the camera type.

This work presented the PSD determination and particle size-based classification of the API. The same high-resolution UV and VIS images allow the system to examine the particle size of MCC. Because the MCC particles are less defined than the API, an advanced method should be applied to identify the edges. In the case of MgSt, due to the small particle size and weight fraction, the application of the machine vision system demands a more comprehensive investigation. In the context of MLX, other excipients or different particle sizes of excipients may not require modified algorithms.

4. CONCLUSION

With the shift towards continuous technologies supported by the regulatory agencies in the pharmaceutical industry, the appropriate sensors, multivariate data analysis, and data-driven methods are becoming more and more valuable. According to that, the newly developed machine vision systems will soon gain more interest in industrial applications. The digital UV/VIS imaging-based particle size classifications supported by the developed image processing algorithms and the applied pattern recognition neural networks were successfully executed with more than 97% accuracy using UV or VIS images. The developed method was

applicable in the case of 2.5 w/w% MLX content, and the application was not restricted to particle size fractions higher or lower than the optimal particle size of the applied API. On the other hand, the particle size analysis based on digital UV and VIS images of the tablets was restricted to those particle size fractions, which D50 value was higher than 5 μm. Although in that case, the defective tablets, which contained fine particles, can be detected, and rejected based on the results of the classification. The particle size analysis of the tablets, when d50 higher than 5 μm was successfully carried out when the mixtures of the API with the target and defected particle size were applied. The presented methods can be feasible for pharmaceutical applications and can open a new perspective for particle size analysis qualitatively and quantitatively based on a single UV or VIS image of an intact tablet.

ACKNOWLEDGEMENT

The presented work was supported by grants from the National Research, Development and Innovation Office of Hungary (grant numbers: KH-129584, FK-132133, PD-121143). The research reported in this paper and carried out at BME has been supported by the National Laboratory of Artificial Intelligence funded by the NRDIO under the auspices of the Ministry for Innovation and Technology. This work was supported by the ÚNKP-21-4 New National Excellence Program of the Ministry for Innovation and Technology from the source of the National Research, Development and Innovation Fund. A. Farkas acknowledges the financial support received through the PREMIUM post-doctorate research program of the Hungarian Academy of Sciences, later Eötvös Loránd Research Network.

REFERENCES

[1] S. S. Gaikwad and S. J. Kshirsagar, "Review on tablet in tablet techniques," *Beni-Suef Univ. J. Basic Appl. Sci.*, vol. 9, no. 1, 2020.

[2] V. Sayeed, "Size, shape, and other physical attributes of generic tablets and capsules - Guidance for Industry," *U.S. Food Drug Adm.*, 2015.

[3] A. L. Skelbæk-Pedersen, T. K. Vilhelmsen, V. Wallaert, and J. Rantanen, "Investigation of the effects of particle size on fragmentation during tableting," *Int. J. Pharm.*, vol. 576, p. 118985, 2020.

[4] M. Kensaku, N. Takuya, H. Koji, and S. Hirakazu, "A large-scale experimental comparison of batch and continuous technologies in pharmaceutical tablet manufacturing using ethenzamide," *Int. J. Pharm.*, vol. 559, pp. 210–219, 2019.

[5] A. Yeaton, "Quality considerations for continuous manufacturing - Guidance for Industry," *U.S. Food Drug Adm.*, 2019.

[6] "Guidance for Industry PAT - A Framework for Innovative Pharmaceutical Development, manufacturing, and Quality Assurance," *U.S. Food Drug Adm.*, 2004.

[7] "Guidance for Industry Q8(R2) Pharmaceutical Development," *U.S. Food Drug Adm.*, 2009.

[8] M. T. am Ende and D. J. am Ende, *Chemical engineering in the pharmaceutical industry : drug product design, development and modeling*. John Wiley & Sons, 2019.

[9] D. M. Scott, A. Boxman, and C. E. Jochen, "In-line particle characterization," *Part. Part. Syst. Charact.*, vol. 15, no. 1, pp. 47–50, 1998.

[10] A. Ramadan, E. B. Basalious, and M. Abdallah, "Industrial application of QbD and NIR chemometric models in quality improvement of immediate release tablets," *Saudi Pharm. J.*, vol. 29, no. 6, pp. 516–526, 2021.

[11] S. Thakral, N. K. Thakral, and R. Suryanarayanan, "Estimation of Drug Particle Size in Intact Tablets by 2-Dimensional X-Ray Diffractometry," *J. Pharm. Sci.*, vol. 107, no. 1, pp. 231–238, 2018.

[12] M. Šimek, V. Grünwaldová, and B. Kratochvíl, "Hot-stage microscopy for determination of API particles in a formulated tablet," *Biomed Res. Int.*, vol. 2014, no. 83245, p. 6, 2014.

[13] S. M. Razavi, M. Gonzalez, and A. M. Cuitiño, "Quantification of lubrication and particle size distribution effects on tensile strength and stiffness of tablets," *Powder Technol.*, vol. 336, pp. 360–374, 2018.

[14] International Council for Harmonisation, "ICH Topic Q4B Annex 12 Analytical Sieving General Chapter Step 3 Annex 12 To Note For Evaluation And Recommendation Of Pharmacopoeial Texts For Use In The ICH Regions On Analytical Sieving General Chapter," 2009.

[15] D. Saravanan, P. Muthudoss, P. Khullar, and A. R. Venis, "Quantitative Microscopy: Particle Size/Shape Characterization, Addressing Common Errors Using 'Analytics Continuum' Approach," *J. Pharm. Sci.*, vol. 110, no. 2, pp. 833–849, Feb. 2021.

[16] K. S. Alexander, J. Azizi, D. Dollimore, and F. A. Patel, "An Interpretation of the Sedimentation Behavior of Pharmaceutical Kaolin and Other Kaolin Preparations in Aqueous Environments," *Drug Dev. Ind. Pharm.*, vol. 15, no. 14–16, pp. 2559–2582, 2008.

[17] A. Gupta, G. E. Peck, R. W. Miller, and K. R. Morris, "Nondestructive measurements of the compact strength and the particle-size distribution after milling of roller compacted powders by near-infrared spectroscopy," *J. Pharm. Sci.*, vol. 93, no. 4, pp. 1047–1053, Apr. 2004.

[18] Q. Zhou, R. Chen, B. Huang, C. Liu, J. Yu, and X. Yu, "An automatic surface defect inspection system for automobiles using machine vision methods," *Sensors 2019, Vol. 19, Page 644*, vol. 19, no. 3, p. 644, 2019.

[19] J. Yu, X. Cheng, L. Lu, and B. Wu, "A machine vision method for measurement of machining tool wear," *Measurement*, vol. 182, p. 109683, 2021.

[20] M. L. Smith, L. N. Smith, and M. F. Hansen, "The quiet revolution in machine vision - a state-of-the-art survey paper, including historical review, perspectives, and future directions," *Comput. Ind.*, vol. 130, p. 103472, 2021.

[21] D. L. Galata *et al.*, "Applications of machine vision in pharmaceutical technology: A review," *Eur. J. Pharm. Sci.*, vol. 159, p. 105717, 2021.

[22] X. Ma *et al.*, "Application of deep learning convolutional neural networks for internal tablet defect detection: high accuracy, throughput, and adaptability," *J. Pharm. Sci.*, vol. 109, no. 4, pp. 1547–1557, 2020.

[23] A. Novikova, J. M. Carstensen, T. Rades, and P. D. C. S. Leopold, "Multispectral UV imaging for surface analysis of MUPS tablets with special focus on the pellet distribution," *Int. J. Pharm.*, vol. 515, no. 1–2, pp. 374–383, Dec. 2016.

[24] I. Kulkov, "The role of artificial intelligence in business transformation: A case of pharmaceutical companies," *Technol. Soc.*, vol. 66, p. 101629, 2021.

[25] K. Mak and M. Pichika, "Artificial intelligence in drug development: present status and future

prospects," *Drug Discov. Today*, vol. 24, no. 3, pp. 773–780, Mar. 2019.

[26] D. Kalyane *et al.*, "Artificial intelligence in the pharmaceutical sector: current scene and future prospect," *Futur. Pharm. Prod. Dev. Res.*, pp. 73–107, Jan. 2020.

[27] F. Marini, "Neural Networks," in *Comprehensive Chemometrics*, vol. 3, Elsevier, 2009, pp. 477–505.

[28] M. B. Butts, J. Hoest-Madsen, and J. C. Refsgaard, "Hydrologic Forecasting," in *Encyclopedia of Physical Science and Technology*, Elsevier, 2003, pp. 547–566.

[29] H. B. Mark, T. H. Martin, and B. D. Howard, *Deep Learning Toolbox™ User's Guide*. 2021.

[30] V. G. Ghorpade and V. S. Koneru, "Pattern recognition neural network model for experimental based compressive strength graded self compacting concrete," in *Materials Today: Proceedings*, 2020, vol. 43, pp. 795–799.

[31] N. Bolourchian, M. Nili, S. M. Foroutan, A. Mahboubi, and A. Nokhodchi, "The use of cooling and anti-solvent precipitation technique to tailor dissolution and physicochemical properties of meloxicam for better performance," *J. Drug Deliv. Sci. Technol.*, vol. 55, p. 101485, 2020.

[32] L. Coppi, M. B. Sanmarti, and M. C. Clavo, "Crystalline forms of meloxicam and processes for their preparation and interconversion," 2005.

[33] L. A. Mészáros *et al.*, "Digital UV/VIS imaging: A rapid PAT tool for crushing strength, drug content and particle size distribution determination in tablets," *Int. J. Pharm.*, vol. 578, p. 119174, 2020.

CRediT Author Statement

Lilla Alexandra Mészáros: Investigation, Methodology, Formal analysis, Writing, Visualization **Attila Farkas:** Conceptualization, Supervision **Lajos Madarász:** Investigation **Rozália Bicsár:** Formal analysis **Dorián László Galata:** Investigation **Brigitta Nagy:** Formal analysis, Investigation **Zsombor Kristóf Nagy:** Conceptualization, Supervision

Declaration of interests

☒ The authors declare that they have no known competing financial interests or personal relationships that could have appeared to influence the work reported in this paper.

☐The authors declare the following financial interests/personal relationships which may be considered as potential competing interests:

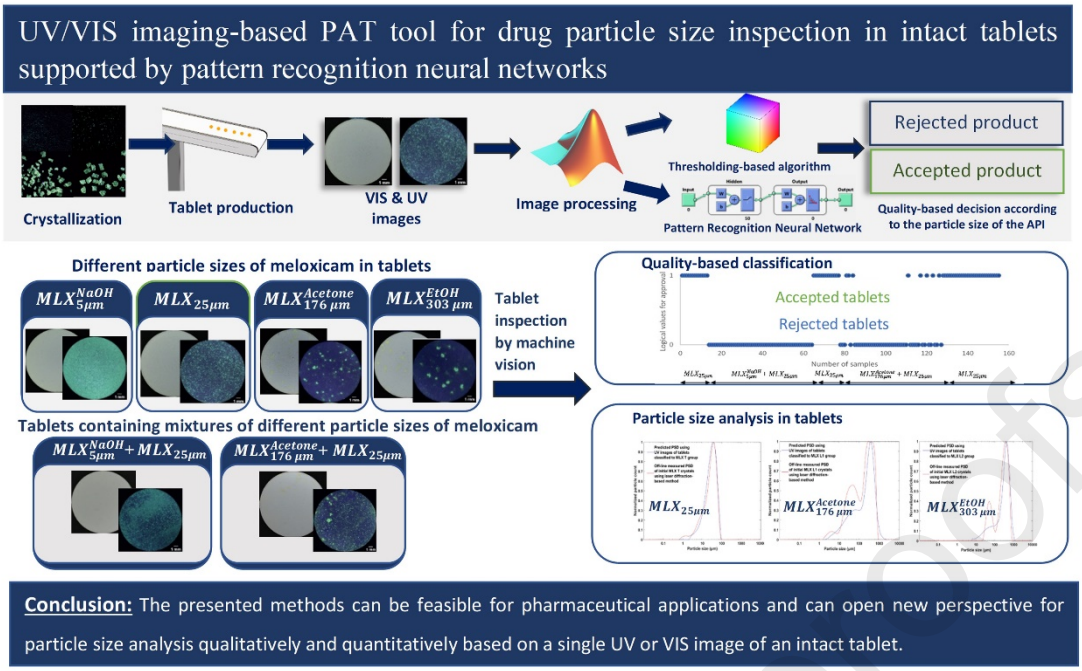

Highlights

- Machine vision recently gained interest in the pharmaceutical industry
- Meloxicam was a model active pharmaceutical ingredient for particle size analysis
- Only an image of a tablet can be applied to extract critical quality attributes
- Image processing and analysis methods were developed for quality monitoring
- Quality-based classification was executed using pattern recognition neural network